This is the Pre-Published Version.

The following publication A. Stepanov, H. Saad, U. Karaagac and J. Mahseredjian, "Initialization of Modular Multilevel Converter Models for the Simulation of Electromagnetic Transients," in IEEE Transactions on Power Delivery, vol. 34, no. 1, pp. 290-300, Feb. 2019 is available at https://dx.doi.org/10.1109/TPWRD.2018.2872883.

Initialization of Modular Multilevel Converter Models for the Simulation of Electromagnetic Transients

Anton Stepanov, *Student Member, IEEE*, Hani Saad, *Member, IEEE*, Ulas Karaagac, *Member, IEEE*, Jean Mahseredjian, *Fellow, IEEE*

***Abstract*—This paper presents an accurate steady-state initialization method for electromagnetic transient (EMT) models of modular multilevel converters (MMCs). The proposed method uses steady-state arm voltages and currents to initialize internal electrical variables and control systems of the converter, including capacitor voltage and gating signals of each sub-module. In addition to typical voltage source converter upper level control, MMC specific controls are also considered, including circulating current control, DC ripple control and capacitor voltage balancing algorithm. EMT simulations on 101-level and 401-level MMC-HVDC systems confirm the accuracy of the proposed method.**

***Index Terms*—High-Voltage Direct Current, initialization, modular multilevel converter, simulation, steady-state**

I. Introduction

Recent trends in voltage source converter HVDC technology include the modular multilevel converter (MMC) topology, shown in Fig. 1. The MMC uses a stack of identical sub-modules (SMs), each providing one step in the resulting multilevel AC waveform. Scalability to higher voltages is easily achieved and reliability is improved by increasing the number of SMs. Other main advantages of the MMC over its conventional two- and three-level counterparts include lower switching frequency, lower losses, lower harmonic content, and lower switching voltage [1], [2]. The MMC technology rapidly gained popularity and several HVDC projects have already been commissioned since 2010, including Trans Bay Cable in America [3], INELFE in Europe [4], and a multi-terminal HVDC grid Nan'ao in China [5].

Electromagnetic transient (EMT) simulations are essential in HVDC connection projects during design and performance assessment stages. As the MMC has a more complicated structure than other types of converters, there is a larger set of models for EMT simulations: the detailed model (DM), detailed equivalent model (DEM), arm equivalent model (AEM) and average value model (AVM) [6], [7]. Depending on the simulated phenomenon and the number of voltage levels in MMC, the EMT converter model can have significant impact on both simulation precision and efficiency [6]-[10]. The DM [6] includes the complete MMC circuit with detailed IGBT representation and offers the ultimate precision. However, its usage causes a significant increase in the size of the main network equations (MNE) and requires refactorization following each IGBT switching operation. The DEM [6], [11] usage improves simulation speed by reducing the size of MNE with Thevenin or Norton equivalent usage for each MMC arm (Fig. 1). DEM accounts for each individual SM circuit and associated control, hence it offers the best precision within the simplified models.

Steady-state initialization of time-domain models of various equipment is essential in EMT type simulations. Depending on the simulated system, lack of steady-state initialization may cause inaccurate simulation results and/or significant increase in computing times due to the duration of initialization transients [12]. As demonstrated in this paper, even lack of only MMC initialization in a realistic AC system results in large initialization transients. Applying disturbance to simulate a specific phenomenon in presence of those transients may trigger protection functions, cause inaccurate results, and/or other unwanted transients. To avoid that, the disturbance should be applied when the initialization transients have decayed below an acceptable level, but at the expense of increased computing (and simulation) time. The cost of this supplementary time can be significant and must be avoided.

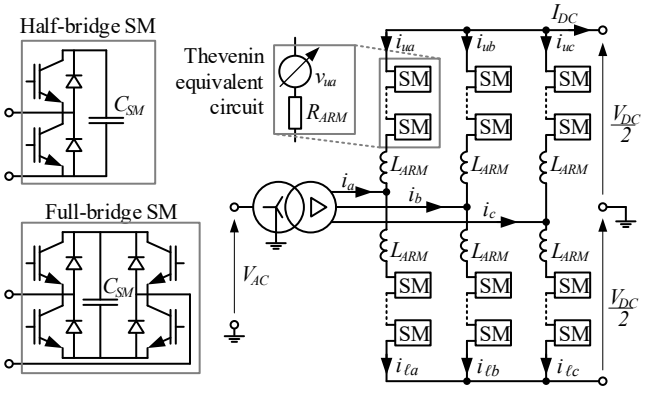

Fig. 1. Typical three-phase MMC topology with a coupling transformer.

A. Stepanov and J. Mahseredjian are with the Department of Electrical Engineering, Polytechnique Montréal, Montreal, QC H3T 1J4, Canada (e-mail: anton.stepanov@polymtl.ca; jeanm@polymtl.ca).

H. Saad is with the Réseau de Transport d'Electricité, Paris 92932, France (e-mail: hani.saad@rte-france.com).

U. Karaagac is with the Department of Electrical Engineering, Hong Kong Polytechnic University, Hung Hom, Kowloon, Hong Kong (e-mail: ulas.karaagac@polyu.edu.hk).

© 2018 IEEE. Personal use of this material is permitted. Permission from IEEE must be obtained for all other uses, in any current or future media, including reprinting/republishing this material for advertising or promotional purposes, creating new collective works, for resale or redistribution to servers or lists, or reuse of any copyrighted component of this work in other works.

Steady-state initialization of detailed MMC models is a challenging task due to model complexity. Accurate steady-state initialization should consider MMC specific controls as well as capacitor voltage and gating signals of each SM. Accurate initialization of MMC models in EMT simulations can provide significant improvement in computation times especially for more detailed models, as they are less time-efficient compared to their simplified counterparts.

To the best knowledge of authors, the existing literature is limited in this area. AC-DC load-flow solution techniques (for example, [13]-[15]) can be used as the first step of the initialization of MMC models, but this has not been discussed. Besides, load-flow techniques usually do not consider internal control system of the converter in detail. Control signals in steady-state analysis of MMCs are considered in [16]-[21], but the authors consider open-loop control (i.e. control signals are known in advance) and/or only the fundamental components in the control system. This is not valid for a typical MMC-HVDC system as it operates under closed-loop control and includes a circulating current suppression control (CCSC) acting on second harmonics. A more advanced steady-state analysis is presented in [22]. However, this paper only demonstrated cases where the 2nd harmonic terms in control signals were known in advance. None of the presented papers considered the initialization of MMCs.

This paper proposes a novel method for steady-state initialization of MMC models which allows to cover virtually all sources of errors causing the initial transients and to initialize MMCs in various conditions. This paper starts in section II with the overview of the initialization process. Section III presents equations for steady-state harmonics of capacitor voltages and switching functions. Section IV deals with the initialization of time-domain variables. EMT simulations of 101-level and 401-level MMC-HVDC systems using DEM and AEM are presented in section V.

II. Overview of the Initialization Process

The proposed initialization method calculates steady-state harmonics of capacitor voltages and control signals based on steady-state arm voltages and currents and initializes internal electrical and control system variables of the MMC model. If large-scale power systems are simulated, an AC-DC load-flow can be used to obtain arm voltages and currents and initialize other models, such as transmission lines, cables, electrical machines, etc., but this is beyond the scope of the paper. In the following, it will be supposed that steady-state arm voltages and currents are known and can be found from a load-flow solution. Therefore, initialization process of a generic EMT study involving MMCs can be presented as follows (Fig. 2):

1. Prerequisites (not discussed in this article):
   1.1. assemble the grid under study in an EMT simulation software (MMCs, transmission lines, cables, machines, etc.);
   1.2. calculate AC-DC load-flow solution considering various control objectives of the converters (active or reactive AC power, DC voltage magnitude, etc.);
   1.3. initialize time-domain models of other elements.
2. MMC initialization. For each MMC in the grid:
   2.1. retrieve arm voltages and currents (DC and fundamental phasors) from the load-flow solution for all six arms;
   2.2. for each arm, find the switching function and total capacitor voltage harmonics using the algorithm of Fig. 3;
   2.3. initialize control system of the MMC based on results from steps 2.1 and 2.2, as explained in the section IV.A;
   2.4. initialize SM voltages based on results from steps 2.1 and 2.2, as shown in the section IV.B.

   Steps 2.1—2.4 can be implemented in the form of user scripts, as it has been done in this paper.

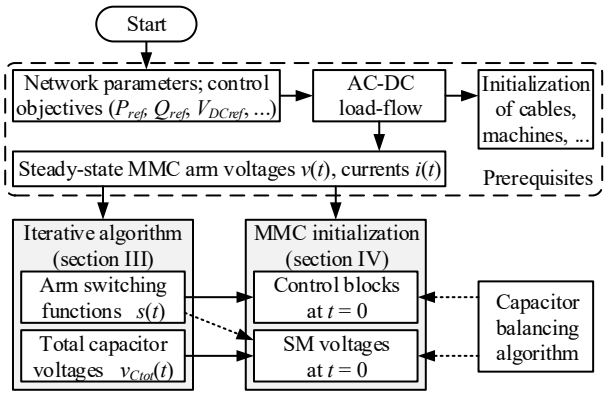

Fig. 2. Proposed procedure for initialization of MMC models. Dashed arrows are for optional unequal SM voltage initialization (see section IV.B).

III. MMC Equations in Steady-State

To correctly initialize MMC models, steady-state analysis must be carried out. The following assumptions are made in this paper for MMC-HVDC systems:

- Generic cascade control system is used [7], achieving perfect reference tracking in steady-state without limit violations.
- CCSC is applied and DC ripple control is present, which is typical in MMC-HVDC transmissions [7], [23].
- High-order harmonics arising from the discrete modular nature of the converter are neglected as they are small in magnitude due to the large number of MMC levels.

With these assumptions, the control system is considered linear and reference values can be used as load-flow constraints. Also, in such a case, arm currents i_{xy} and voltages v_{xy} (Fig. 1) contain only DC and fundamental components. In balanced conditions, the DC components of i_{xy} are equal to $-I_{DC}/3$, and those of v_{xy} are equal to $V_{DC}/2$ minus the voltage drop on the arm resistance R_{ARM} (includes ON-state IGBT resistances [6]). Up to the second-order harmonics will be considered for the total capacitor voltage $v_{Ctot_{xy}}$ (i.e. the sum of all capacitor voltages in the arm), for the arm switching function s_{xy} and for the charging current $i_{Ctot_{xy}}$ [6] (the subscripts $x = u, \ell$ denoting upper/lower arms and $y = a, b, c$ denoting phases, will be omitted for clarity):

$$v(t) = v_0(t) + v_1(t) = V_0 + V_1 \cos(\omega t + \varphi_{v1}) \quad (1)$$

$$i(t)=i_0(t)+i_1(t)=I_0+I_1\cos(\omega t+\varphi_{i1}) \quad (2)$$

$$i_{Ctot}(t)=i_{Ctot1}(t)+i_{Ctot2}(t)= =I_{Ctot1}\cos(\omega t+\varphi_{ic1})+I_{Ctot2}\cos(2\omega t+\varphi_{ic2}) \quad (3)$$

$$v_{Ctot}(t)=v_{Ctot0}(t)+v_{Ctot1}(t)+v_{Ctot2}(t)= =V_{Ctot0}+V_{Ctot1}\cos(\omega t+\varphi_{vc1})+V_{Ctot2}\cos(2\omega t+\varphi_{vc2}) \quad (4)$$

$$s(t)=s_0(t)+s_1(t)+s_2(t)= =S_0+S_1\cos(\omega t+\varphi_{s1})+S_2\cos(2\omega t+\varphi_{s2}) \quad (5)$$

where the subscripts 0, 1 and 2 denote the zero-, first- and second-order harmonics amplitudes, respectively, ω is the grid frequency in rad/s, and φ_z is the angle of any variable z in radians.

The following steady-state equations hold for each MMC arm [6], [19]:

$$v(t)=v_{Ctot}(t)\,s(t) \quad (6)$$

$$i_{Ctot}(t)=i(t)\,s(t) \quad (7)$$

$$v_{Ctot\,n}(t)=\frac{1}{C_{eq}}\int i_{Ctot\,n}(\tau)\,d\tau \quad (8)$$

where the subscript n denotes the n[th] harmonic (except zero), $C_{eq}=C_{SM}/N_{SM}$ is the equivalent capacitance, C_{SM} is SM capacitance, and N_{SM} is the number of SMs per arm.

This paper proposes an iterative solution approach for to obtain the steady-state harmonics in (4) and (5). The details of the algorithm are presented in the following subsections. This paper uses the complex notation, i.e. $Z\cos(\omega t+\varphi_z)\rightarrow Z\angle\varphi_z\rightarrow\overline{Z}$.

A. Equations for the Iterative Algorithm

Since for each MMC arm it is necessary to find up to the second harmonic terms of the total capacitor voltage (4) and arm switching function (5), in total there are nine unknowns: complex variables representing harmonics contain real and imaginary parts and the DC component of the switching function is known (taken as $S_0=0.5$), see Table I. So, the following system of nine equations is proposed:

$$\overline{V_{Ctot1}}=\frac{1}{j\omega C_{eq}}\left[\overline{I_1}S_0+I_0\overline{S_1}+\frac{1}{2}\overline{I_1^*}\,\overline{S_2}\right] \quad (9)$$

$$\overline{V_{Ctot2}}=\frac{1}{j2\omega C_{eq}}\left[I_0\overline{S_2}+\frac{1}{2}\overline{I_1}\,\overline{S_1}\right] \quad (10)$$

$$\overline{S_1}=\frac{1}{V_{Ctot0}}\left[\overline{V_1}-S_0\overline{V_{Ctot1}}-\frac{1}{2}\overline{S'^*_1}\,\overline{V_{Ctot2}}-\frac{1}{2}\overline{S_2}\,\overline{V_{Ctot1}}\right] \quad (11)$$

$$V_{Ctot0}=\frac{1}{S_0}\left[V_0-\frac{1}{2}\mathrm{Re}\left(\overline{V_{Ctot1}}\,\overline{S_1^*}+\overline{V_{Ctot2}}\,\overline{S_2^*}\right)\right] \quad (12)$$

$$\overline{S_2}=-\frac{1}{V_{Ctot0}}\left[S_0\overline{V_{Ctot2}}+\frac{1}{2}\overline{S_1}\,\overline{V_{Ctot1}}\right] \quad (13)$$

The derivation of these equations based on (1)-(8) is presented in the appendix A. In (9), (11), and (12) the asterisk represents complex conjugation. This system of equations is nonlinear and unknown quantities can be found on both left and right sides of all the equations.

TABLE I
ARM VARIABLES USED IN THE ITERATIVE ALGORITHM

Variable	Type	Symbol
Unknown variables		
Total capacitor voltage DC component	Real	V_{Ctot0}
Total capacitor voltage fundamental	Complex	$\overline{V_{Ctot1}}$
Total capacitor voltage second harmonic	Complex	$\overline{V_{Ctot2}}$
Arm switching function fundamental	Complex	$\overline{S_1}$
Arm switching function second harmonic	Complex	$\overline{S_2}$
Known variables		
Arm current DC component	Real	I_0
Arm current fundamental	Complex	$\overline{I_1}$
Arm voltage DC component	Real	V_0
Arm voltage fundamental	Complex	$\overline{V_1}$
Arm switching function DC component	Real	S_0

B. Solution and Initial Approximation

Different methods can be used to solve equations (9)-(13), the iterative method implemented in this paper is shown in Fig. 3. At each iteration, unknown variables are successively refined by recalculating (9)-(13) one by one (fixed-point iterations). The initial guess is found as:

$$V_{Ctot0}\approx 2V_0 \quad (14)$$

$$\overline{S_1}\approx\frac{V_1}{2V_0}\angle\varphi_{v1} \quad (15)$$

$$\overline{S_2}\approx 0\angle 0 \quad (16)$$

With this, (9) and (10) can be calculated, which in turn allows to calculate (11) and (12) etc. Although in (11) $\overline{S_1}$ can also be seen in the right-hand side, its value can be taken from the previous iteration, which is shown as $\overline{S'_1}$.

At the end of each iteration, the amplitude errors ε_Z and the angle errors ε_φ for any variable z are calculated using

$$\varepsilon_Z=\frac{\left|Z^k-Z^{k-1}\right|}{\left[Z^k+Z^{k-1}\right]/2} \quad (17)$$

$$\varepsilon_\varphi=\frac{\left|\varphi_z^k-\varphi_z^{k-1}\right|}{2\pi} \quad (18)$$

where k is the iteration count.

The algorithm stops when the maximum error for all variables ε_{MAX} is below a predefined tolerance ε. In practical realizations, a limit can be set on the maximum number of iterations k_{MAX}. Since high-order harmonics are not considered in (1)-(5), the tolerance limit was set to $\varepsilon=10^{-5}$, higher precision is unnecessary. In all performed tests under various conditions sufficient precision has been obtained in no more than five iterations.

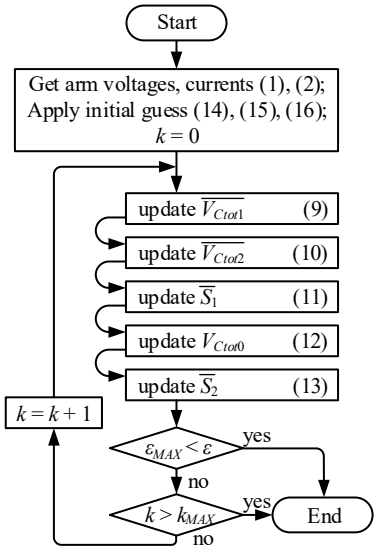

Fig. 3. Algorithm for obtaining steady-state arm values.

IV. MMC Station Initialization

Once the steady-state harmonics of $v_{Ctot}(t)$ and $s(t)$ have been calculated for all six arms, the control system of the MMC and SM voltages can be initialized.

A. Control System Initialization

The unbalance between upper and lower arms is disregarded in steady-state operation. Consequently, the output signals of AC current regulators, CCSC, and DC ripple controls can be found by applying Fortescue, Clarke or Park transformations to the appropriate harmonics of the three-phase control signals. AC current regulators use the fundamentals (11), and circulating current controls use the second harmonics (13).

The considered generic cascade control system consists of linear regulators [7], [23] due to perfect reference tracking assumption. Hence, only the integral parts of the controllers must be initialized as the contributions of proportional terms are equal to zero. Hereafter, the subscripts "ref" and "meas" are used for the reference and measured values, respectively.

1) Proportional-Integral Current Control

PI controllers in dq reference frame are used for the AC side primary current control and CCSC. For the primary current control, AC side currents can be obtained from arm currents with KCL. Output signals s_d^+ and s_q^+ can be obtained by applying Park transformation matrix $[P(t)]$ to the fundamentals of arm switching functions (11). In balanced conditions:

$$\left[s_d^+ \quad s_q^+\right]^T = k_{pu}\left[P(t)\right]\left[s_{1la}(t) \quad s_{1lb}(t) \quad s_{1lc}(t)\right]^T \quad (19)$$

where k_{pu} is added to adjust for the p.u. control system.

Finally, history terms of the integral blocks of the positive sequence AC current regulator in dq frame H_d^+ and H_q^+ (Fig. 4) can be initialized as:

$$H_d^+ = s_d^+ + L_\Sigma \omega i_q^+ \quad (20)$$

$$H_q^+ = s_q^+ - L_\Sigma \omega i_d^+ \quad (21)$$

where $L_\Sigma = L_{TRFO} + L_{ARM}/2$ is the AC side equivalent, L_{ARM} is the arm and L_{TRFO} is the transformer inductance; i_d^+, i_q^+ are the positive sequence AC side currents in dq reference frame.

History terms of the negative sequence AC side current control and CCSC can be found using the same approach.

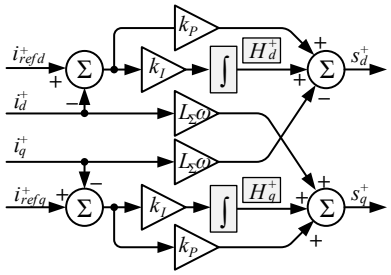

Fig. 4. PI current controller in positive dq frame with initialization.

2) Proportional-Resonant Current Control

Proportional-Resonant controllers $S_{PR}(p)$ are used for primary AC current control, CCSC and DC ripple control [23]:

$$S_{PR}(p) = \left[I_{ref}(p) - I_{meas}(p)\right]\left[k_P + \frac{k_R p}{p^2 + \omega^2}\right] \quad (22)$$

where p is the Laplace variable; $I_{meas}(p)$ and $I_{ref}(p)$ are the Laplace transforms of the measured and reference currents in αβ frame; $k_P = S_P(p)$ and $k_R p / \left[p^2 + \omega^2\right] = S_R(p)$ are the proportional and the resonant branches respectively.

Contribution of the proportional branch equals zero in steady-state due to perfect reference tracking, so only the resonant branch is initialized. It can be implemented as a combination of two integrals (Fig. 5) based on the following equation, as demonstrated in the appendix B:

$$S_R(p) = \frac{1}{p}\left[k_R\left[I_{ref}(p) - I_{meas}(p)\right] - \frac{1}{p}\omega^2 S_R(p)\right] \quad (23)$$

In steady-state, the output of a PR regulator is described by a generic cosine function $s_R(t) = s_{PR}(t) = S_{PR}\cos(\omega t + \varphi_{PR})$ which can be obtained by applying Clarke transformation similarly to (19). In this case, history terms of the integrals $H1$ and $H2$ (Fig. 5) are obtained as follows: it can be seen that the output of one integral ($H1$) is connected to the output of the regulator, so since the proportional term is disregarded:

$$H1(t) = s_{PR}(t) = S_{PR}\cos(\omega t + \varphi_{PR}) \quad (24)$$

The output of the other integral ($H2$) can be obtained as the input (i.e. derivative) of the first integral with a minus sign:

$$H2(t) = -\frac{d}{dt}H1(t) = \omega S_{PR}\sin(\omega t + \varphi_{PR}) \quad (25)$$

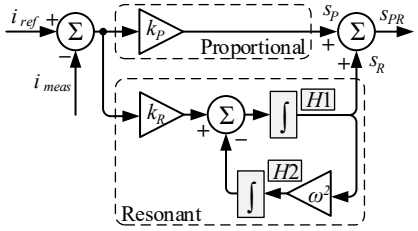

Fig. 5. Proportional-Resonant current controller implementation suitable for initialization.

3) Outer Control

The outer controls consist of PI regulators and produce the reference values for the inner AC side current controller. The active current channel is used to control either active power (P) or DC voltage (V_{DC}), and the reactive current channel is used to control either reactive power (Q) or AC voltage (V_{AC}). When the reference distribution strategies are considered [23], [24], history values of the corresponding integrals (H_P, $H_{V_{DC}}$, H_Q, $H_{V_{AC}}$) are defined by the average active (P_{PCC}) and reactive (Q_{PCC}) powers at the point of common coupling (PCC):

$$H_P = H_{V_{DC}} = P_{PCC} = v_d^+ i_d^+ + v_q^+ i_q^+ + v_d^- i_d^- + v_q^- i_q^- \quad (26)$$

$$H_Q = H_{V_{AC}} = Q_{PCC} = v_q^+ i_d^+ - v_d^+ i_q^+ + v_q^- i_d^- - v_d^- i_q^- \quad (27)$$

where v_d^+, v_q^+, v_d^-, v_q^- are the voltages and i_d^+, i_q^+, i_d^-, i_q^- are the currents at the PCC in positive and negative dq frames.

In case of nominal PCC voltage, history terms in (26) and (27) will be equal in p.u. to the positive sequence currents i_d^+ and i_q^+, respectively.

4) PLL

In steady-state, the frequency is equal to its nominal value and the PLL is perfectly synchronized. Hence, the initial phase angle of the PLL (Θ_{PLL}) can be calculated from the positive sequence PCC voltage in αβ frame v_α^+ and v_β^+:

$$\Theta_{PLL}(t) = \text{atan2}\left(v_\beta^+(t), v_\alpha^+(t)\right) \quad (28)$$

5) SM Level Control

The number of SMs to be inserted N_{ins} can be calculated using either the control system or electrical circuit variables:

$$N_{ins}(t) = \text{round}\left(N_{SM}\ s(t)\right) \quad (29)$$

$$N_{ins}(t) = \text{round}\left(N_{SM}\ v(t) / v_{Ctot}(t)\right) \quad (30)$$

As SM level control has an immediate action, there is no history term to initialize. If all SMs have the same initial capacitor voltage, CBA can select SMs in any order for the first time-step (sequentially, uniformly), in any case a transient is inevitable because SM voltages are not exactly equal to each other and are constantly changing their values due to arm current. The initial selection will not have any impact on the simulation results because all SMs are identical. However, if uniform capacitor voltage distribution is considered (as per section IV.B.2), the SMs should be inserted uniformly to minimize transients.

B. SM Capacitor Voltage

For accurate initialization, it is necessary to provide initial voltage for each SM if detailed models are used. Several initialization approaches are considered.

1) Equal SM Voltages

The easiest approach is initializing all SMs with the same capacitor voltage value which is equal to the average value:

$$v_{SM_j}(t) = v_{Ctot}(t) / N_{SM} \quad (31)$$

where j = 1, 2, …, N_{SM} is the SM index.

However, this leads to a short initial transient in the simulation because the SM voltages in the arm are not actually equal, even though MMCs have a control block dedicated to balancing SM voltages near the average value. This is discussed in the next subsection.

2) SM Voltages with NLC CBA

Accurate initialization needs to account for the voltage difference among SMs introduced by the capacitor balancing algorithm (CBA). Several CBAs exist, and each can have a different impact on the distribution of SM voltages. The permutation-based Nearest Level Control (NLC) CBA is considered here for demonstration purposes [25]. A permutation is the insertion of the SM with the lowest voltage and bypassing of the SM with the highest voltage at each time-step (with charging arm current, opposite otherwise).

The following assumptions are made for the CBA:

- Uniform distribution of SM voltages around average value;
- SMs are inserted when their voltage is the lowest and bypassed when their voltage is the highest in the arm (with charging arm current, opposite otherwise);
- Inserted SMs are distributed uniformly by their voltage.

Additional assumptions are made for the simulation:

- The simulation time-step Δt is sufficiently small to assume that the arm current and the number of inserted SMs do not change for several time-steps;
- All SMs are in the same conditions regarding negative insertion in steady-state: if SMs are only inserted positively, presented calculations are valid for hybrid MMCs with any number of half-bridge (HB) and full-bridge (FB) SMs [2]. If SMs need to be inserted negatively at some periods, presented calculations will only be valid for MMC arms with only FB-SMs, since HB-SMs would be all bypassed during these periods, i.e. the uniformity would be broken.

In such conditions, it is sufficient to know the maximum excursion of SM voltage around the average value (denoted as ΔV) to obtain individual SM voltages. To find ΔV, the concept of insertion time $T_{ins}(t)$ is introduced: the SMs are kept inserted for $T_{ins}(t)$ around time t. With the small time-step assumption, the insertion time can be obtained:

$$T_{ins}(t) = \Delta t\ N_{ins}(t) / N_{perm} \quad (32)$$

where N_{perm} is the number of permutations per time-step.

In the simulations with relatively larger time-steps, the precision of T_{ins} in (32) can be improved by deducing the equivalent number of permutations per time-step

$$N_{perm}(t) \approx N_0 + \left|\frac{N_{add}(t)}{2}\right| \approx N_0 + \Delta t \left|\frac{d}{dt} s(t)\right| \frac{N_{SM}}{2} \quad (33)$$

where N_0 is the constant number of permutations per time-step as defined by the CBA and N_{add} is the number of added SMs (negative if SMs are removed). It is divided by two to get the equivalent number of permutations, because only one SM is affected, whereas the permutation acts on two SMs.

The passing arm current charges inserted SMs; so the voltage change of one SM during $T_{ins}(t)$ can be calculated as:

$$\Delta v_{SM}(t) = \frac{1}{C_{SM}} \int_{t-T_{ins}/2}^{t+T_{ins}/2} i(\tau)\, d\tau \approx \frac{i(t)\, T_{ins}(t)}{C_{SM}} \quad (34)$$

and the change in the average value of SM voltage in the arm can be written as:

$$\frac{\Delta v_{Ctot}(t)}{N_{SM}} = \frac{1}{N_{SM} C_{eq}} \int_{t-T_{ins}/2}^{t+T_{ins}/2} i_{Ctot}(\tau)\, d\tau \approx \frac{i(t)\, s(t)\, T_{ins}(t)}{C_{SM}} \quad (35)$$

Maximum excursion of SM voltage around the average value can be found as the difference between (34) and (35):

$$\Delta V(t) = \Delta v_{SM}(t) - \frac{\Delta v_{Ctot}(t)}{N_{SM}} \approx \frac{i(t)\left[1 - s(t)\right] T_{ins}(t)}{C_{SM}} \quad (36)$$

Finally, the initial SM voltages can be expressed as:

$$v_{SM_j}(t) = \frac{v_{Ctot}(t)}{N_{SM}} + \Delta V(t) \left[\frac{j-1}{N_{SM}-1} - \frac{1}{2} \right] \quad (37)$$

3) SM Voltages with PWM-based Control

Another type of SM-level control is based on Pulse-Width Modulation (PWM), including phase-shift PWM (PS-PWM), phase-disposition PWM and others [26]. Although PWM-based controls are usually applied for the MMCs with a relatively low number of levels, which are out of the scope of this article, the proposed initialization procedure is still applicable. If PS-PWM control is considered, equations (34)–(37) are valid, but the insertion time $T_{ins}(t)$ should be calculated differently. If the PWM frequency f_{PWM} is several times higher than the grid frequency,

$$T_{ins}(t) = s(t) / f_{PWM} \quad (38)$$

It has been reported that without additional measures PWM-based control can cause voltage imbalance [26], [27], therefore, similarly to [28], a simple sorting algorithm can be added that selects the most appropriate SMs to insert or to bypass when the number of SMs changes.

C. Delays

If the EMT simulation software solves control and power system equations simultaneously, the above initialization procedures are sufficient to avoid initialization transients. However, there can be a one-time-step delay between the solution of control and power system equations. Additional delays can be present when external code is referenced in the form of a dynamic-link library (DLL).

To counteract the presence of these delays and minimize their effects on initialization, it is proposed to extrapolate the final control references (i.e. arm switching functions) by one time-step for each delay present in the control loop:

$$s_E(t) \approx s(t) + m\, \Delta t \frac{ds(t)}{dt} \approx \left[m+1\right] s(t) - m\, s(t - \Delta t) \quad (39)$$

where s_E is the extrapolated signal; m is the number of time-steps to extrapolate.

V. Simulation Results

The initialization method developed in this paper can be implemented in any EMT-type simulation tool using available external programming interfaces. In this paper, it was implemented and tested in EMTP [29] using a DLL interface.

The simulated network is a point-to-point symmetrical monopole hybrid MMC-HVDC link with 101 levels (Fig. 6). The DEM is used for both MMCs. The control system includes PR controllers for AC side currents, CCSC and DC ripple suppression. MMC1 controls active and reactive powers, MMC2 controls DC voltage and reactive power. Other system parameters are given in Table II. DC cable model details can be found in [6].

The convergence of the algorithm proposed in section III is shown in Fig. 7 for phase-A upper arm variables of MMC1. All the variables gradually converge to an accurate solution. The values at the fifth iteration are used for the initialization of MMCs (section IV) because the maximum relative error ε_{MAX} is below 10^{-5}. The initial values calculated in section IV and supplied to the EMT models were obtained using $t = 0$.

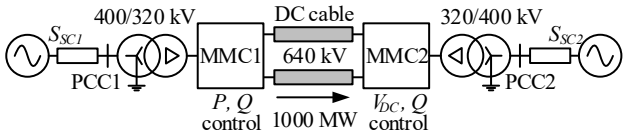

Fig. 6. Simulated point-to-point MMC-HVDC link.

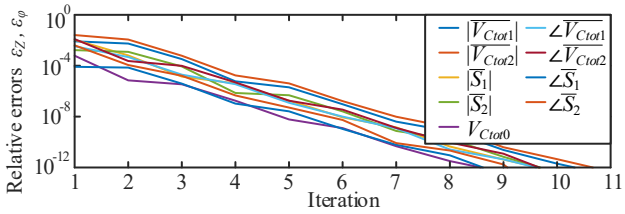

Fig. 7. Convergence of the proposed algorithm for phase-A upper arm values at MMC1 (see (17), (18)).

TABLE II
Simulation Parameters

Parameter	Nominal value	Symbol
Simulation time-step	20 µs	Δt
Grid frequency (both grids)	$2\pi \times 50$ rad/s	ω
Grid voltage (both grids)	400 kV	V_{AC}
Grid short-circuit level (both grids)	10 GVA	S_{SC}
DC voltage	640 kV	V_{DC}
Nominal converter power (both stations)	1000 MW	
Number of SMs per arm (HB / FB)	100 (20 / 80)	N_{SM}
Active power reference	1 pu	P_{ref}
Reactive power reference (both stations)	0 pu	Q_{ref}
DC voltage reference	1 pu	V_{DCref}
(ON / OFF)-resistance of IGBTs & Diodes	1 mΩ / 1 MΩ	
Arm inductance	0.15 pu	L_{ARM}
Transformer inductance	0.18 pu	L_{TRFO}
Capacitor energy	40 kJ/MVA	
Permutations per time-step	1	N_0

A. External Behavior

The external behavior of the converter is evaluated from the DC voltage and current of MMC1 (PQ-control station) in Fig. 8. The fully initialized converter operates in steady-state conditions from the first time-point. On the other hand, it takes more than 0.5 s of simulation time to reach steady-state when starting with zero initial conditions (i.e. without performing steady-state analysis and initializing the simulated circuit).

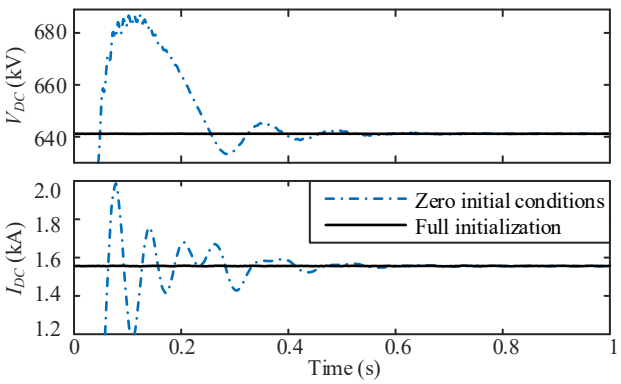

Fig. 8. DC voltage and current at MMC1 terminals during initial transient.

B. Capacitor Voltage

The total capacitor voltage $v_{Ctot}(t)$ of phase-A upper arm at MMC1 and its average value during initial transient are shown in Fig. 9. In the presented simulations, the initial values of the capacitor voltages are calculated considering zero-; zero- and first-; zero-, first- and second-order harmonics (see (4)). As seen from Fig. 9, all three harmonic components need to be considered to eliminate the initialization transient.

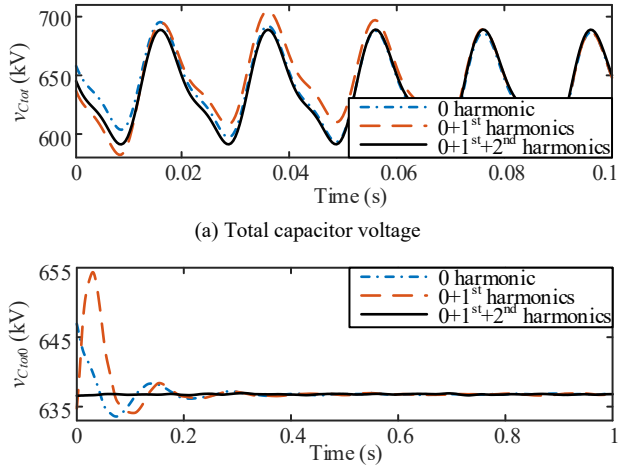

(a) Total capacitor voltage

(b) Average value of the total capacitor voltage

Fig. 9. Phase-A upper arm total capacitor voltage at MMC1 when initializing with 0; 0 and 1st; 0, 1st and 2nd order harmonics of v_{Ctot} (4).

C. Control System

The switching function $s(t)$ of phase-A upper arm at MMC1 and its average value are shown in Fig. 10. It is the signal before NLC (nearest level control [7]). Therefore, the differences due to the finite number of levels do not appear. Similar to the previous section, initial values of the arm switching functions (and, consequently, initial history terms of integrals, section IV.A) supplied to the time-domain simulation are calculated considering zero-; zero- and first-; zero-, first- and second-order harmonics (see (5)). All three harmonic components must be considered to eliminate the initialization transient.

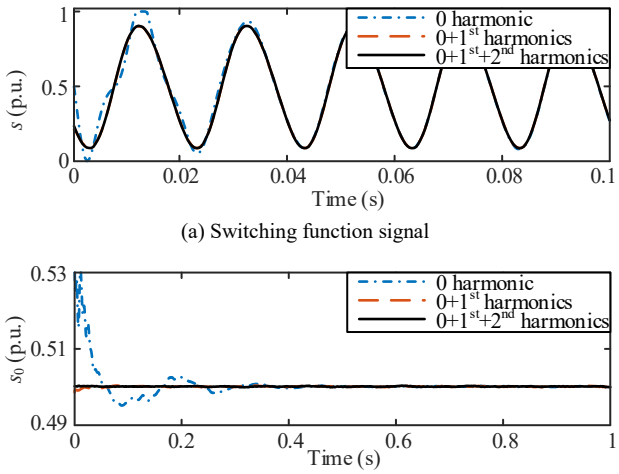

(a) Switching function signal

(b) Average value of the switching function signal

Fig. 10. Phase-A upper arm switching function at MMC1 when initializing with 0; 0 and 1st; 0, 1st and 2nd order harmonics of s (5).

D. SM Level Initialization

While the effect of unequal SM voltage can hardly be seen outside the converter, its effect is clearly visible on the arm level. The deviations from the average voltage value for all capacitors in phase-A upper arm at MMC1, as well as the maximum excursion of SM voltages (36), are shown in Fig. 11. With the equal initial SM voltage assumption (31), an initial transient is seen within the first 5 ms (Fig. 11, upper part). No transient is seen in the case with the initial uniform voltage distribution of (37) (see Fig. 11, lower part). Also, the results confirm the accuracy of SM voltage excursion ΔV (36).

Fig. 12 shows how the inserted SMs are distributed in the arm according to their voltages. Although the distribution of SMs is not perfectly uniform in steady-state, as shown in Fig. 12.a (adjacent SMs are inserted, up to 10 adjacent SMs are bypassed), the initial uniform distribution case in Fig. 12.b can be considered as an adequate approximation. Equal initial SM voltage assumption (Fig. 12.c) produces incorrect results. As explained in subsection IV.A.5, the distribution of inserted SMs in the beginning of the simulation will be as shown in Fig. 12.c, if all SMs initially have the same voltage (31), irrespective of the initial selection by the CBA.

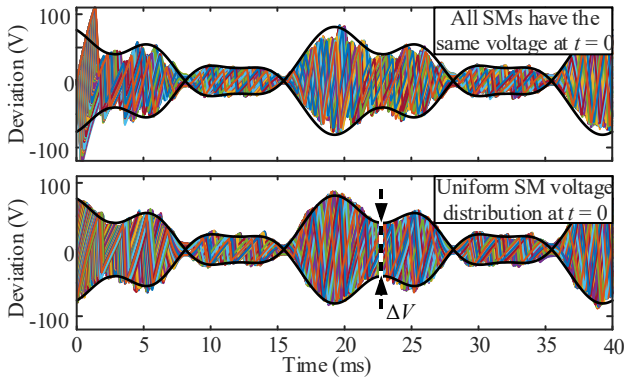

Fig. 11. Deviations from the average voltage value for all SMs in phase-A upper arm at MMC1 (black curves are obtained using (36)).

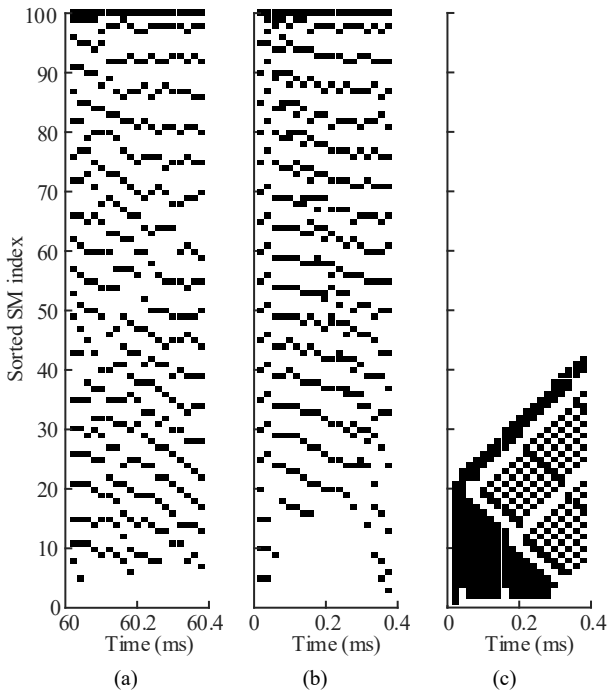

Fig. 12. SM indices according to voltage sorting (index 1 – lowest voltage, index 100 – highest voltage). Black rectangles represent inserted SMs. (a) indices of inserted SMs after three cycles; (b) initial uniform distribution of inserted SMs is considered, SM voltages are obtained using (37); (c) initial distribution of inserted SMs is neglected, SM voltages are obtained using (31).

E. Extrapolation

To demonstrate the effects of extrapolation proposed in section IV.C, a 401-level MMC-HVDC with 360 FB SMs and 40 HB SMs is now used in Fig. 6 with $\Delta t = 5$ µs.

The initial DC voltage of MMC1 is shown in Fig. 13 (due to the voltage drop along the DC cable caused by the 1 GW power flow, its value is higher than 640 kV). An initialization transient lasting about 0.2 s can be seen if the extrapolation is omitted. To suppress the transient, a two-time-step extrapolation (39) is applied in the case of DEM (Fig. 13, left part). One time-step covers the delay between the power circuit solution and the control system solution, the other time-step compensates for the delay caused by the implementation of the CBA using a DLL.

In the case of AEM (Fig. 13, right), only the delay between the power circuit solution and the control system solution is present, because the CBA DLL is not included in this model (individual SM voltages are not available). Therefore, only one-time-step extrapolation can be applied to remove the initial transient.

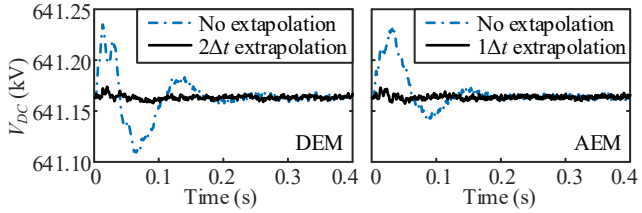

Fig. 13. Effect of extrapolation on DC voltage at MMC1 terminals.

F. Time Gains

1) Test-case 1

To evaluate the computing/simulation time reduction resulting from the proposed initialization method, 1% DC voltage reference step is applied at MMC2 when the system reaches steady-state (same 401-level DEM system is used). The DC voltage at MMC2 terminals with and without initialization is shown in Fig. 14. Without initialization, small oscillations remaining from the initial transient are still visible before the step change (Fig. 14, left). If these oscillations are neglected, the system is in steady-state at $t = 0.6$ s. With proper initialization, the test can be performed near simulation startup (Fig. 14, right).

Transient behavior in both simulations is identical, but the results are obtained faster when initialization is applied because less simulation time is necessary: the CPU time in the test case without initialization is 136.6 s (for 1 s of simulation time). The CPU time in the test case with initialization is 59.2 s (for 0.4 s of simulation time). The time needed to perform initialization of the MMCs with the proposed method is negligible (around 20 milliseconds). Thus, the proposed initialization saves more than 50% of computing time.

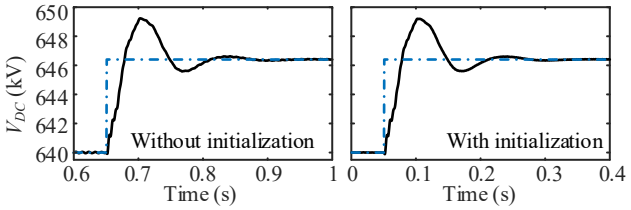

Fig. 14. DC voltage at MMC2 terminals. Dash-dot line is the reference signal.

2) Test-case 2

The second test system is shown in Fig. 15: two 400 kV AC systems are connected through a 101-level HB-MMC HVDC link modeled using AEM. MMC1 controls active and reactive powers, MMC2 controls DC and AC voltage amplitudes. The system connected to MMC1 is represented with its Thevenin equivalent. The AC system connected to MMC2 is developed using a practical system from [30]. Synchronous machine subnetworks contain detailed machine models with controls and transformers. Loads are modeled by constant impedances. Lines are represented by distributed constant parameter models and coupled pi-sections (PI1–PI3). AC-DC load-flow is calculated and all elements of the AC grid are initialized. Once the system reaches steady-state, a single-line-to-ground fault is applied at ALIAG bus end of the ALIAG-SOMA line and is cleared with 0.1 s delay by isolating the line.

Fig. 16 shows that initialization transients die out in around 3 s without HVDC link initialization, although all other system components are initialized correctly ($t = 0$ is the time of the fault). The initialization transient is longer compared to the previous test case due to synchronous machine rotor oscillations (it can be noted that HVDC link variables, such as DC voltage etc., stabilize faster due to fast feedback control). Fig. 17 shows that with the proposed HVDC link initialization, the fault can be applied 20 ms after simulation startup and 3 s of simulation time (57.6 s of CPU time) can be eliminated.

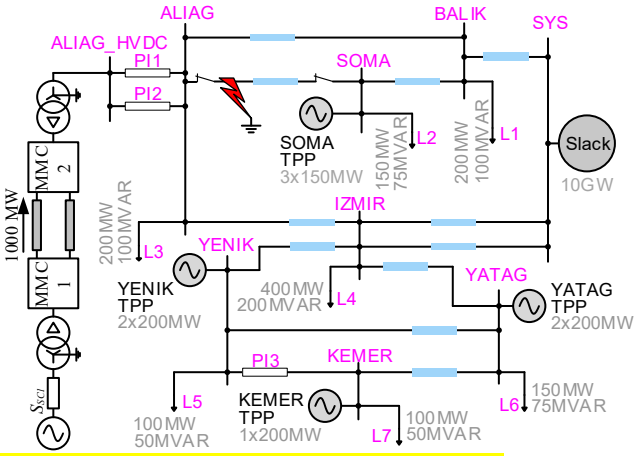

Fig. 15. Simulated small-scale AC grid with an HVDC link.

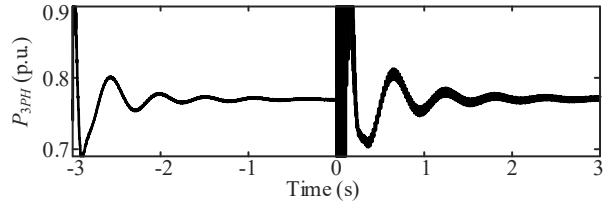

Fig. 16. SOMA TPP active power output without HVDC link initialization.

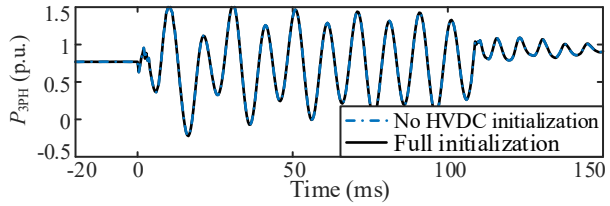

Fig. 17. SOMA TPP active power output with and without HVDC link initialization (fault instants are shifted to $t = 0$ s).

VI. Conclusion

This paper presents an accurate steady-state initialization method for the EMT-type simulation of MMCs. The proposed method uses steady-state arm voltages and currents to obtain steady-state harmonics of total capacitor voltages and arm switching functions for all six arms of the MMC. It initializes electrical and control system variables of various MMC models, including individual capacitor voltages and gating signals of each SM. The MMC specific controls are considered, as well as the typical upper level control.

The accuracy of the proposed method is validated through the EMT simulations of 101-level and 401-level MMC-HVDC test systems using DEM and AEM of MMC. In the simulated cases, lack of initialization caused large initial transients that took more than 0.5 s of simulation time to decay. Simulation results also demonstrated that elimination of the initial transient can be achieved only with an initialization approach that considers zero-, first-, and second-order harmonics in the system. The equal initial SM voltage assumption causes a short initial transient in the simulations; despite its marginal impact, the SM capacitors should be initialized considering capacitor balancing algorithm to eliminate this initial transient. The presence of delays between the solutions of power and control system equations can also cause extraneous transients which can be eliminated using extrapolation. The computing time to perform initialization calculations is negligible compared to the time needed to converge to the steady-state solution without initialization.

Appendix

A. Derivation of the Equations for the Iterative Algorithm

1) Capacitor Voltage Fundamental Component

The fundamental term of the total capacitor voltage ($\overline{V_{Ctot1}}$) can be obtained from the fundamental term of the charging current i_{Ctot1} [16]. From (2)-(5), (7) and (8):

$$i_{Ctot1}(t) = I_{Ctot1}\cos(\omega t + \varphi_{ic1}) = I_1 S_0 \cos(\omega t + \varphi_{i1}) + \\ + I_0 S_1 \cos(\omega t + \varphi_{s1}) + \frac{1}{2} I_1 S_2 \cos(\omega t + \varphi_{s2} - \varphi_{i1}) \quad (40)$$

$$\overline{I_{Ctot1}} = \overline{I}_1 S_0 + I_0 \overline{S}_1 + \frac{1}{2}\overline{I}_1^* \overline{S}_2 \quad (41)$$

$$\overline{V_{Ctot1}} = \frac{\overline{I_{Ctot1}}}{j\omega C_{eq}} = \frac{1}{j\omega C_{eq}}\left[\overline{I}_1 S_0 + I_0 \overline{S}_1 + \frac{1}{2}\overline{I}_1^* \overline{S}_2\right] \quad (42)$$

2) Capacitor Voltage Second Harmonic

Using a similar formulation, the second harmonic of the total capacitor voltage ($\overline{V_{Ctot2}}$) can be written as:

$$i_{Ctot2}(t) = I_{Ctot2}\cos(2\omega t + \varphi_{ic2}) = I_0 S_2 \cos(2\omega t + \varphi_{s2}) + \\ + \frac{1}{2} I_1 S_1 \cos(2\omega t + \varphi_{i1} + \varphi_{s1}) \quad (43)$$

$$\overline{V_{Ctot2}} = \frac{\overline{I_{Ctot2}}}{j2\omega C_{eq}} = \frac{1}{j2\omega C_{eq}}\left[I_0 \overline{S}_2 + \frac{1}{2}\overline{I}_1 \overline{S}_1\right] \quad (44)$$

3) Switching Function Fundamental Component

The fundamental component of the switching function ($\overline{S_1}$) can be calculated from the equation of the arm voltage fundamental v_1:

$$v_1(t) = V_{Ctot0} S_1 \cos(\omega t + \varphi_{s1}) + S_0 V_{Ctot1}\cos(\omega t + \varphi_{c1}) + \\ + \frac{S_1 V_{Ctot2}}{2}\cos(\omega t + \varphi_{vc2} - \varphi_{s1}) + \frac{S_2 V_{Ctot1}}{2}\cos(\omega t + \varphi_{s2} - \varphi_{vc1}) \quad (45)$$

In (45), S_1 and φ_{s1} contribute to two summands. The multiplication with the second harmonic of capacitor voltage produces much smaller impact on the final value of $v_1(t)$. Hence, for this summand the values can be taken from the previous iteration (shown as $\overline{S'_1}$ in (46)). Finally, $\overline{S_1}$ is

$$\overline{S_1} = \frac{1}{V_{Ctot0}}\left[\overline{V_1} - S_0 \overline{V_{Ctot1}} - \frac{1}{2}\overline{S'^*_1}\,\overline{V_{Ctot2}} - \frac{1}{2}\overline{S_2}\,\overline{V_{Ctot1}}\right] \quad (46)$$

4) Capacitor Voltage DC Component

The DC component of capacitor voltage (V_{Ctot0}) can be calculated from the DC component of the arm voltage v_0:

$$v_0(t) = V_0 = V_{Ctot0}\, S_0 + \frac{1}{2} V_{Ctot1}\, S_1 \cos(\varphi_{vc1} - \varphi_{s1}) + \\ + \frac{1}{2} V_{Ctot2}\, S_2 \cos(\varphi_{vc2} - \varphi_{s2}) \quad (47)$$

$$V_{Ctot0}=\frac{1}{S_0}\left[V_0-\frac{1}{2}\mathrm{Re}\left(\overline{V_{Ctot1}}\,\overline{S_1}^{*}+\overline{V_{Ctot2}}\,\overline{S_2}^{*}\right)\right] \quad (48)$$

5) Switching Function Second Harmonic

The second harmonic of the switching function ($\overline{S_2}$) can be calculated from the second harmonic of the arm voltage v_2, which equals zero due to CCSC and DC ripple control.

$$v_2(t)=0=S_0V_{Ctot2}\cos\left(2\omega t+\varphi_{vc2}\right)+$$
$$+V_{Ctot0}S_2\cos\left(2\omega t+\varphi_{s2}\right)+\frac{1}{2}S_1V_{Ctot1}\cos\left(2\omega t+\varphi_{vc1}+\varphi_{s1}\right) \quad (49)$$

$$\overline{S_2}=-\frac{1}{V_{Ctot0}}\left[S_0\overline{V_{Ctot2}}+\frac{1}{2}\overline{S_1}\overline{V_{Ctot1}}\right] \quad (50)$$

B. Derivation of Proportional-Resonant Controller

Resonant part of a PR controller (22) in Laplace domain is:

$$S_R(p)=U(p)\,k_R\,\frac{p}{p^2+\omega^2} \quad (51)$$

where $U(p)=I_{ref}(p)-I_{meas}(p)$. Multiplying both sides of (51) by $\left[p^2+\omega^2\right]/p^2$ yields:

$$S_R(p)+S_R(p)\frac{\omega^2}{p^2}=\frac{1}{p}U(p)\,k_R \quad (52)$$

By rearranging the terms, we obtain

$$S_R(p)=\frac{1}{p}\left[U(p)\,k_R-\frac{1}{p}S_R(p)\omega^2\right] \quad (53)$$

which is the same as (23). Finally, knowing that $1/p$ in (53) is the Laplace transform of an integral, the implementation shown in Fig. 5 can be easily obtained.

REFERENCES

[1] A. Lesnicar and R. Marquardt, "An innovative modular multilevel converter topology suitable for a wide power range," in *2003 IEEE Bologna PowerTech*, Bologna, Italy, 2003, pp. 272-277.

[2] W. Lin, D. Jovcic, S. Nguefeu and H. Saad, "Full-Bridge MMC Converter Optimal Design to HVDC Operational Requirements," *IEEE Trans. Power Del.,* vol. 31, pp. 1342-1350, Jun 2016.

[3] S. P. Teeuwsen, "Modeling the Trans Bay Cable Project as Voltage-sourced Converter with Modular Multilevel Converter design," *IEEE PES General Meeting*, Detroit, Michigan, USA, 2011.

[4] S. Dennetière, H. Saad, B. Clerc, and J. Mahseredjian, "Setup and performances of the real-time simulation platform connected to the INELFE control system," *Electric Power Systems Research*, vol. 138, pp. 180-187, Sep. 2016.

[5] Z. Li, F. Gao, F. Xu, X. Ma, Z. Chu, P. Wang, *et al.*, "Power module capacitor voltage balancing method for a±350-kV/1000-MW modular multilevel converter," *IEEE Trans. Power Electron.,* vol. 31, pp. 3977-3984, 2016.

[6] H. Saad, S. Dennetiere, J. Mahseredjian, P. Delarue, X. Guillaud, J. Peralta, *et al.*, "Modular Multilevel Converter Models for Electromagnetic Transients," *IEEE Trans. Power Del.,* vol. 29, pp. 1481-1489, Jun. 2014.

[7] H. Saad, J. Peralta, S. Dennetiere, J. Mahseredjian, J. Jatskevich, J. A. Martinez, *et al.*, "Dynamic Averaged and Simplified Models for MMC-Based HVDC Transmission Systems," *IEEE Trans. Power Del.,* vol. 28, pp. 1723-1730, Jul. 2013.

[8] CIGRE Working Group B4.57, "Guide for the Development of Models for HVDC Converters in a HVDC Grid," Paris, Dec. 2014.

[9] U. Karaagac, J. Mahseredjian, L. Cai and H. Saad, "Offshore Wind Farm Modeling Accuracy and Efficiency in MMC-based Multi-Terminal HVDC Connection," *IEEE Trans. Power Del.*, vol. 32, no. 2, pp. 617-627, April 2017.

[10] L. Cai, U. Karaagac and J. Mahseredjian, "Simulation of Startup Sequence of an Offshore Wind Farm with MMC-HVDC Grid Connection," *IEEE Trans. Power Del.*, vol. 32, no. 2, pp. 638-646, April 2017.

[11] U. N. Gnanarathna, A. M. Gole, and R. P. Jayasinghe, "Efficient Modeling of Modular Multilevel HVDC Converters (MMC) on Electromagnetic Transient Simulation Programs," *IEEE Trans. Power Del.,* vol. 26, pp. 316-324, Jan 2011.

[12] J. Mahseredjian, I. Kocar and U. Karaagac, "Solution Techniques for Electromagnetic Transients in Power Systems," in Transient Analysis of Power Systems: Solution Techniques, Tools and Applications, Wiley-IEEE Press, 2015, pp. 9-36.

[13] C. Runze, Z. Baohui, D. Jingming, H. Zhiguo, and Z. Tao, "Unified Power Flow Algorithm Based on the NR Method for Hybrid AC/DC Grids Incorporating VSCs," *IEEE Trans. Power Syst.,* vol. 31, pp. 4310-18, 2016.

[14] W. Wenyuan and M. Barnes, "Power Flow Algorithms for Multi-Terminal VSC-HVDC With Droop Control," *IEEE Trans. Power Syst.,* vol. 29, pp. 1721-30, 2014.

[15] M. Baradar and M. Ghandhari, "A Multi-Option Unified Power Flow Approach for Hybrid AC/DC Grids Incorporating Multi-Terminal VSC-HVDC," *IEEE Trans. Power Syst.,* vol. 28, pp. 2376-83, 2013.

[16] X. Shi, Z. Wang, B. Liu, Y. Li, L. M. Tolbert, and F. Wang, "Steady-State Modeling of Modular Multilevel Converter under Unbalanced Grid Conditions," *IEEE Trans. Power Electron.,* vol.32, pp. 7306-7324, 2017.

[17] Y. Zhou, D. Jiang, J. Guo, P. Hu, and Y. Liang, "Analysis and Control of Modular Multilevel Converters Under Unbalanced Conditions," *IEEE Trans. Power Del.,* vol. 28, pp. 1986-1995, 2013.

[18] K. Ilves, A. Antonopoulos, S. Norrga, and H.-P. Nee, "Steady-state analysis of interaction between harmonic components of arm and line quantities of modular multilevel converters," *IEEE Trans. Power Electron.,* vol. 27, pp. 57-68, 2012.

[19] Q. Song, W. Liu, X. Li, H. Rao, S. Xu, and L. Li, "A steady-state analysis method for a modular multilevel converter," *IEEE Trans. Power Electron.,* vol. 28, pp. 3702-3713, 2013.

[20] D. Wu and L. Peng, "Analysis and suppressing method for the output voltage harmonics of modular multilevel converter," *IEEE Trans. Power Electron.,* vol. 31, pp. 4755-4765, 2016.

[21] X. Li, Q. Song, W. Liu, S. Xu, Z. Zhu, and X. Li, "Performance analysis and optimization of circulating current control for modular multilevel converter," *IEEE Trans. Ind. Electron.,* vol. 63, pp. 716-727, 2016.

[22] J. Wang, J. Liang, F. Gao, X. Dong, C. Wang, and B. Zhao, "A Closed-Loop Time-Domain Analysis Method for Modular Multilevel Converter," *IEEE Trans. Power Electron.,* vol. 32, pp. 7494-7508, 2017.

[23] A. Stepanov, H. Saad, J. Mahseredjian, and A. Wataré, "Overview of Generic HVDC-MMC Control under Unbalanced Grid Conditions," *IPST 2017*, Seoul, South Korea, 2017.

[24] R. Teodorescu, M. Liserre, and P. Rodriguez, *Grid converters for photovoltaic and wind power systems*: John Wiley and Sons, Ltd., 2011.

[25] H. Saad, "Modélisation et simulation temps réel d'une liaison HVDC de type VSC-MMC," PhD Thesis, Département de génie électrique, École Polytechnique de Montréal, Monteal, Canada, 2015.

[26] S. Debnath, J. Qin, B. Bahrani, M. Saeedifard and P. Barbosa, "Operation, Control, and Applications of the Modular Multilevel Converter: A Review," in *IEEE Transactions on Power Electronics*, vol. 30, no. 1, pp. 37-53, Jan. 2015.

[27] Q. Tu, Z. Xu and L. Xu, "Reduced Switching-Frequency Modulation and Circulating Current Suppression for Modular Multilevel Converters," in *IEEE Transactions on Power Delivery*, vol. 26, no. 3, pp. 2009-2017, July 2011.

[28] M. Saeedifard and R. Iravani, "Dynamic Performance of a Modular Multilevel Back-to-Back HVDC System," in *IEEE Transactions on Power Delivery*, vol. 25, no. 4, pp. 2903-2912, Oct. 2010.

[29] J. Mahseredjian, S. Dennetière, L. Dubé, B. Khodabakhchian and L. Gérin-Lajoie, "On a new approach for the simulation of transients in power systems," *Electric Power Systems Research*, vol. 77, issue 11, pp. 1514-1520, Sep. 2007.

[30] U. Karaagac, J. Mahseredjian and O. Saad, "An efficient synchronous machine model for electromagnetic transients", IEEE Trans. on Power Delivery, vol. 26, no. 4, pp. 2456-2465, Oct. 2011.